

Extracting higher central charge from a single wave function

Ryohei Kobayashi,^{1,*} Taige Wang,^{2,3} Tomohiro Soejima,² Roger S. K. Mong,⁴ and Shinsei Ryu⁵

¹*Department of Physics, Condensed Matter Theory Center, and Joint Quantum Institute, University of Maryland, College Park, Maryland 20742, USA*

²*Department of Physics, University of California, Berkeley, California 94720 USA*

³*Material Science Division, Lawrence Berkeley National Laboratory, Berkeley, CA 94720, USA*

⁴*Department of Physics and Astronomy, University of Pittsburgh, Pittsburgh, PA 15260, USA*

⁵*Department of Physics, Princeton University, Princeton, New Jersey, 08544, USA*

(Dated: March 10, 2023)

A (2+1)D topologically ordered phase may or may not have a gappable edge, even if its chiral central charge c_- is vanishing. Recently, it is discovered that a quantity regarded as a “higher” version of chiral central charge gives a further obstruction beyond c_- to gapping out the edge. In this Letter, we show that the higher central charges can be characterized by the expectation value of the *partial rotation* operator acting on the wavefunction of the topologically ordered state. This allows us to extract the higher central charge from a single wavefunction, which can be evaluated on a quantum computer. Our characterization of the higher central charge is analytically derived from the modular properties of edge conformal field theory, as well as the numerical results with the $\nu = 1/2$ bosonic Laughlin state and the non-Abelian gapped phase of the Kitaev honeycomb model, which corresponds to $U(1)_2$ and Ising topological order respectively. The letter establishes a numerical method to obtain a set of obstructions to the gappable edge of (2+1)D bosonic topological order beyond c_- . We also point out that the expectation values of the partial rotation on a single wavefunction put a constraint on the low-energy spectrum of the bulk-boundary system of (2+1)D bosonic topological order, reminiscent of the Lieb-Schultz-Mattis type theorems.

Introduction – (2+1)D topological phases with bulk energy gap host various intriguing physical phenomena [1]. One of the most striking is the phenomenon of bulk-edge correspondence, where the property of the bulk heavily constrains what can happen at the boundary of the system. The most celebrated example is the case of Integer Quantum Hall effect (IQHE), where nonzero bulk Chern number implies the presence of gapless charged edge modes [2]. Even in the absence of charge conservation, systems with nonzero chiral central charge, which signals nonzero *thermal* Hall conductance, has gapless edge modes [3]. We have a good theoretical understanding of these quantities by way of coarse-grained Chern-Simons theory, and we can extract them from microscopic wavefunctions via entanglement measures [4–7].

In the presence of anyonic excitations, there are properties beyond chiral central charge c_- that enforces the presence of gapless edge modes. In many cases, nontrivial braiding statistics between anyons can present an obstruction to gapping out all anyonic degrees of freedom simultaneously at the edge of the system [8, 9]. Such phases of matter are said to have an *ungappable* edge. Recently, it is discovered that a quantity called *higher central charge* can partially capture “ungappability” of the edge [10, 11]. In particular, higher central charges of an Abelian topological order completely determines whether it has an ungappable edge [12]. However, so far the quantity has been characterized purely through the topological quantum field theory (TQFT) framework, and a microscopic understanding of the higher central charge has been lacking.

In this Letter, we show that the expectation value of the *partial rotation* operator – rotation operator that acts only on a part of the system – can be used to reliably extract the higher central charge of topologically ordered systems. This is the first proposal that relates the wavefunction of a topological ordered state to its higher central charges, and our operational definition even allows its evaluation on a quantum computer. Our finding is supported by an analytical conformal field theory (CFT) calculation, as well as numerical simulation of the non-Abelian phase of the Kitaev honeycomb model and $\nu = 1/2$ bosonic Laughlin state. This Letter establishes a general numerical method to obtain a set of obstructions to a gappable edge of a bosonic topological order beyond c_- .

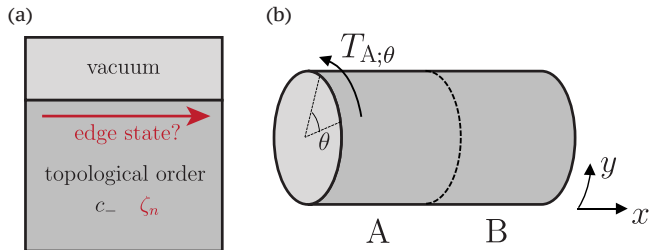


FIG. 1. (a) The setup for which we considered the gappability problem. The obstruction can be captured by the chiral central charge c_- and higher central charge ζ_n . (b) Schematics of the partial rotation of a cylinder bisected into A and B subsystems.

Definition and properties of higher central charge – The higher central charges ζ_n are complex numbers characterizing a topologically ordered state, labeled by a positive integer n . The higher central charge can be easily

* E-mail: ryok@umd.edu

computed from the properties of anyons in the topological order. Concretely, for a given bosonic (2+1)D topologically ordered state, the higher central charge is defined as the following phase

$$\zeta_n = \frac{\sum_a d_a^2 \theta_a^n}{|\sum_a d_a^2 \theta_a^n|}, \quad (1)$$

where the sum is over all anyons in the topological order. d_a is quantum dimension, and θ_a is topological twist (i.e., self-statistics) of an anyon a . When $n = 1$, ζ_1 reduces to the Gauss sum formula for chiral central charge of the bosonic topological phase modulo 8, $\zeta_1 = e^{\frac{2\pi i}{8} c_-}$, hence ζ_n formally provides a generalization of c_- .

Higher central charges put a constraint on the gappability of the edge; it was proven in [10] that $\zeta_n = 1$ for all n such that $\gcd(n, N_{\text{FS}}) = 1$ give necessary conditions for admitting a gapped boundary. Here, N_{FS} is called the Frobenius-Schur exponent, which is defined as the smallest positive integer such that $\theta_a^{N_{\text{FS}}} = 1$ for all anyons a . For example, $U(1)_2 \times U(1)_{-4}$ Chern-Simons theory has $\zeta_3 = -1$, which shows that the topological order does not admit a gapped boundary even though $c_- = 0$. For (2+1)D bosonic Abelian topological phases one can also derive sufficient conditions: the higher central charges $\{\zeta_n\}$ for $\gcd(n, \frac{N_{\text{FS}}}{\gcd(n, N_{\text{FS}})}) = 1$ give both necessary and sufficient conditions for a gappable boundary [12].

Main result – To extract the higher central charges from a single wavefunction, we consider a (2+1)D topological ordered phase located on a cylinder. The state on the cylinder is labeled by the anyon a , which corresponds to a quasiparticle obtained by shrinking the puncture at the end of the cylinder. Suppose that we have realized a ground state $|\Psi\rangle$ on the cylinder labeled by the trivial anyon 1. Let us then take a bipartition of the cylinder into the two subsystems labeled by A and B, and write the translation operator for the A subsystem by the angle θ along the circumference as $T_{A;\theta}$ (see Fig. 1). We then find that the following quantity extracts the higher central charge ζ_n ,

$$\mathcal{T}_1\left(\frac{2\pi}{n}\right) := \langle \Psi | T_{A;\frac{2\pi}{n}} | \Psi \rangle \propto e^{-2\pi i (\frac{2}{n} + n) \frac{c_-}{24}} \times \sum_a d_a^2 \theta_a^n, \quad (2)$$

where \propto in this Letter always means being proportional up to a positive real number. In the special case where $n = 1$, the rhs becomes 1 since $\sum_a d_a^2 \theta_a \propto e^{\frac{2\pi i}{8} c_-}$, which is consistent with the fact that the rotation by 2π acting on the cylinder A gives an identity operator. For $n > 1$ and $\gcd(n, N_{\text{FS}}) = 1$, the above rhs becomes proportional to the higher central charge ζ_n and gives information about a non-trivial obstruction to gapped boundary beyond c_- . Since c_- can be extracted from a single wavefunction [4, 13], our method allows a complete characterization of all higher central charges.

Analytic derivation – Eq. (2) can be derived by employing the cut-and-glue approach established in [14, 15], which describes the entanglement spectrum of the A subsystem in the long wavelength by that of the (1+1)D

CFT on its edges. Namely, the reduced density matrix for the A subsystem is effectively given by $\rho_A = \rho_{A;l} \otimes \rho_{A;r}$, where $\rho_{A;l}, \rho_{A;r}$ denote the CFTs on the left and right edges respectively. The left edge lies at the end of the whole cylinder that realizes the ground state of CFT; the right edge of the A subsystem entangled with the B subsystem is described by a thermal density matrix of a perturbed edge CFT within the fixed topological sector [16]. The form of the perturbation in the entanglement Hamiltonian is not universal. In the calculations to follow, we assume that the entanglement Hamiltonian is that of the unperturbed CFT: $\rho_{A;r} = e^{-\beta_r H_r}$, and check the validity of this assumptions with our numerics.

Since the operator $T_{A;\theta}$ acts as the translation of the CFT on the boundary, the expectation value of $T_{A;2\pi/n}$ for the A subsystem is evaluated in terms of the translation of edge CFTs. The partial rotation is then expressed in terms of CFT partition functions as

$$\begin{aligned} \mathcal{T}_1\left(\frac{2\pi}{n}\right) &= \frac{\text{Tr}[e^{iP_l \frac{L}{n}} e^{-\frac{\xi_l}{v} H_l}] \text{Tr}[e^{iP_r \frac{L}{n}} e^{-\frac{\xi_r}{v} H_r}]}{\text{Tr}[e^{-\frac{\xi_l}{v} H_l}] \text{Tr}[e^{-\frac{\xi_r}{v} H_r}]} \\ &= \frac{\chi_1\left(\frac{i\xi_l}{L} + \frac{1}{n}\right) \chi_1\left(\frac{i\xi_r}{L} - \frac{1}{n}\right)}{\chi_1\left(\frac{i\xi_l}{L}\right) \chi_1\left(\frac{i\xi_r}{L}\right)}, \end{aligned} \quad (3)$$

where we introduced the velocity v of the CFT, correlation length $\xi_l = v\beta_l$, $\xi_r = v\beta_r$, and the circumference of the cylinder L . P_l and P_r are translation operators on the left and right edge $P_l = -\frac{1}{v}H_l$, $P_r = \frac{1}{v}H_r$. $\chi_1(\tau)$ is the CFT character of the trivial topological sector with modular parameter τ . In our setup where $L \ll \xi_l$, the characters for the left edge are approximated as

$$\chi_1\left(\frac{i\xi_l}{L}\right) \approx e^{\frac{2\pi\xi_l}{L} \frac{c_-}{24}}, \quad \chi_1\left(\frac{i\xi_l}{L} + \frac{1}{n}\right) \approx e^{\frac{2\pi\xi_l}{L} \frac{c_-}{24}} e^{-\frac{2\pi i}{n} \frac{c_-}{24}}. \quad (4)$$

Meanwhile, the edge CFT at the right edge cutting the system has high temperature $L \gg \xi_r$. The characters for the right edge can be approximately computed by performing proper modular S, T transformations as [17]

$$\begin{aligned} \chi_1\left(\frac{i\xi_r}{L}\right) &= \sum_a S_{1,a} \chi_a\left(\frac{iL}{\xi_r}\right) \approx \frac{1}{\mathcal{D}} e^{\frac{2\pi L}{\xi_r} \frac{c_-}{24}}, \\ \chi_1\left(\frac{i\xi_r}{L} - \frac{1}{n}\right) &= \sum_a (ST^n S)_{1,a} \chi_a\left(\frac{iL}{n^2 \xi_r} + \frac{1}{n}\right) \\ &\approx (ST^n S)_{1,1} e^{-\frac{2\pi i}{n} \frac{c_-}{24}} e^{\frac{2\pi L}{n^2 \xi_r} \frac{c_-}{24}} \\ &= \frac{1}{\mathcal{D}^2} e^{-2\pi i (n + \frac{1}{n}) \frac{c_-}{24}} e^{\frac{2\pi L}{n^2 \xi_r} \frac{c_-}{24}} \sum_a d_a^2 \theta_a^n, \end{aligned} \quad (6)$$

where n is assumed to be a small positive integer satisfying $n^2 \ll L/\xi_r$. The sum is over the anyons a that labels the conformal block of the edge CFT, and $\mathcal{D} = \sqrt{\sum_a d_a^2}$ is the total quantum dimension. By combining the above approximations of the characters, $\mathcal{T}_1(2\pi/n)$ in Eq. (3) is expressed in the form of Eq. (2).

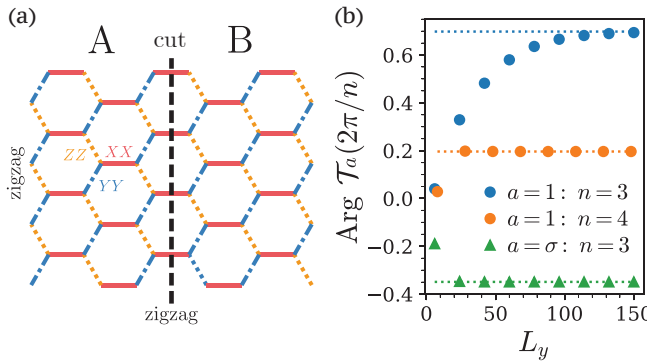


FIG. 2. (a) Geometry of the Kitaev model on a cylinder. Red solid lines, blue dotted-dashed lines, and yellow dotted lines correspond to X , Y and Z type Ising interactions, respectively. The lattice is periodic in the y direction, and has the zigzag boundary condition in the x direction. (b) The partial rotations $T_a(2\pi/n)$ evaluated in the Ising topological phase of the Kitaev model at $n = 3, 4$. The σ sector at $n = 4$ is not shown since partial rotation results in zero expectation value. We used $J_x = J_y = J_z = 1$, $\kappa = 0.1$ for computation.

A similar computation can be performed when the ground state $|\Psi\rangle$ lives in a generic topological sector labeled by an anyon of the topological order,

$$T_a\left(\frac{2\pi}{n}\right) \propto e^{\frac{2\pi i}{n}h_a - 2\pi i(\frac{2}{n}+n)\frac{c_-}{24}} \times \sum_b S_{ab} d_b \theta_b^n, \quad (7)$$

where $T_a(2\pi/n) := \langle \Psi_a | T_{A;2\pi/n} | \Psi_a \rangle$ with $|\Psi_a\rangle$ being the ground state in the topological sector labeled by an anyon a . We define twisted higher central charge

$$\zeta_{n,a} := \sum_b S_{ab} d_b \theta_b^n, \quad (8)$$

which is proportional to higher central charge when $a = 1$, $\zeta_{n,1} = (\sum_b d_b \theta_b^n)/\mathcal{D}$. The derivation of Eq. (7) is relegated to Supplemental Materials.

While the definition of the quantity Eq. (2) is akin to that of the momentum polarization in the large n limit introduced in Ref. [18, 19], we emphasize that the partial rotation by the finite angle $T_a(2\pi/n)$ extracts a completely different universal quantity from the momentum polarization. Indeed, the momentum polarization with $n \rightarrow \infty$ does not depend on the higher central charge, which is expressed as

$$\lim_{n \rightarrow \infty} T_a\left(\frac{2\pi}{n}\right) \propto \exp\left[\frac{2\pi i}{n}\left(h_a - \frac{c_-}{24} - \frac{c_-}{24}\frac{L^2}{\xi_r^2}\right)\right]. \quad (9)$$

Remarkably, while the momentum polarization Eq. (9) depends on the circumference L and the non-universal correlation length ξ_r , Eq. (2) solely gives a constant universal value as the combination of c_- and higher central charge. In Supplemental Materials, we describe how the behavior of the partial rotation interpolates between higher central charge and momentum polarization by increasing n from a small positive integer to infinity.

sector a	$\zeta_{n,a}$	$T_a\left(\frac{2\pi}{n}\right)$
Ising	$e^{\frac{2\pi i}{16}}, e^{\frac{2\pi i}{16}}, e^{\frac{6\pi i}{16}}, e^{\frac{4\pi i}{16}}$	$1, 1, e^{\frac{2\pi i}{9}}, e^{\frac{\pi i}{16}}$
	$1, 0, 1, 0$	$1, 0, e^{-\frac{\pi i}{9}}, 0$
$U(1)_2$	$e^{\frac{2\pi i}{8}}, 0, e^{-\frac{2\pi i}{8}}, 1$	$1, 0, e^{\frac{13\pi i}{9}}, e^{\frac{13\pi i}{8}}$
	$e^{-\frac{2\pi i}{8}}, 1, e^{\frac{2\pi i}{8}}, 0$	$1, 1, e^{\frac{\pi i}{9}}, 0$

TABLE I. The phases of $\zeta_{n,a}$ and the partial rotation $T_a\left(\frac{2\pi}{n}\right)$ for $n = 1, 2, 3, 4$ in each topological sector of Ising and $U(1)_2$. We write 0 when the magnitude is vanishing.

Numerical results – We demonstrate the validity of the formula Eq. (2) for two examples: the Ising topological order realized by the Kitaev honeycomb model, and the $U(1)_2$ topological order realized by the $\nu = 1/2$ bosonic Laughlin state. Their $\zeta_{n,a}$ and expected values of the partial rotation $T_a(2\pi/n)$ are summarized in Table I. For some of the n 's in a given topological sector, the magnitude of T_1 might vanish. However, this could only occur when $\text{gcd}(n, N_{\text{FS}}) \neq 1$, which therefore does not obscure the examination of whether the topological order has a gappable boundary.

The Kitaev honeycomb model is defined on a honeycomb lattice with a qubit on each vertex, with the Hamiltonian given by

$$H = J_x \sum_{\langle ij \rangle \in \text{R edge}} X_i X_j + J_y \sum_{\langle ij \rangle \in \text{B edge}} Y_i Y_j + J_z \sum_{\langle ij \rangle \in \text{Y edge}} Z_i Z_j + \kappa \sum_{\langle ijk \rangle} X_i Y_j Z_k, \quad (10)$$

where the last term is a time-reversal breaking term introduced by turning on magnetic field, which realizes the non-Abelian gapped phase [20]. The non-Abelian phase is known to host Ising topological order with anyons $1, \sigma, \psi$ with topological twists $\theta_1 = 1$, $\theta_\sigma = e^{2\pi i/16}$, $\theta_\psi = -1$.

To compute partial rotation, we employ a cylinder geometry. The cylinder is terminated with zigzag boundary condition on both ends as depicted in Fig. 2, and we act on the left half of system with partial rotation.

The model is equivalent to a system of free Majorana fermions coupled to dynamical \mathbb{Z}_2 gauge field, by rewriting the spin degrees of freedom using Majorana fermion operators c , which act as dynamical free Majorana fermions, and b , which describes the \mathbb{Z}_2 gauge field.

As demonstrated in Supplemental Materials, the partial rotation for the state on the cylinder lying in the trivial sector can be expressed as

$$T_1\left(\frac{2\pi}{n}\right) \propto \text{Tr}\left(\frac{1 + (-1)^F}{2} e^{-H_E} T_{A; \frac{2\pi}{n}}\right), \quad (11)$$

where H_E is the entanglement Hamiltonian for the free fermion state in the A subsystem with the fixed flat \mathbb{Z}_2 gauge field, with the boundary condition in y direction taken to be anti-periodic. The operator $(1 + (-1)^F)/2$ gives a projector onto the Hilbert space with even

fermion parity. Following Ref. [18], one can further evaluate it from the entanglement spectrum of the free Majorana fermions:

$$\begin{aligned} \mathcal{T}_1\left(\frac{2\pi}{n}\right) \propto \prod_{m,k_y} & \left[\frac{1+e^{ik_y L_y/n}}{2} + \frac{1-e^{ik_y L_y/n}}{2} \tanh \frac{\xi_{mk_y}}{2} \right] \\ & + \prod_{m,k_y} \left[\frac{1-e^{ik_y L_y/n}}{2} + \frac{1+e^{ik_y L_y/n}}{2} \tanh \frac{\xi_{mk_y}}{2} \right] \end{aligned} \quad (12)$$

where ξ_{mk_y} is the entanglement spectrum for H_E , carried by a quasiparticle with momentum k_y in y direction. Analogously, the partial rotation for the σ sector is expressed in terms of the entanglement Hamiltonian H_E^σ given by setting the periodic boundary condition in y direction, $\mathcal{T}_\sigma(2\pi/n) \propto \text{Tr}(e^{-H_E^\sigma} T_{A;2\pi/n})$, which can also be computed from entanglement spectrum of H_E^σ .

We show the result of this evaluation for $1, \sigma$ sectors in Fig. 2. We see that $\text{Arg}(\mathcal{T}_a(2\pi/n))$ converges to predicted values. We only present for $n \geq 3$ and $|\mathcal{T}_a(2\pi/n)| > 0$. $\mathcal{T}_a(2\pi/n)$ is always real (no phase) for $n = 1$ and 2 since the phase part exactly cancels.

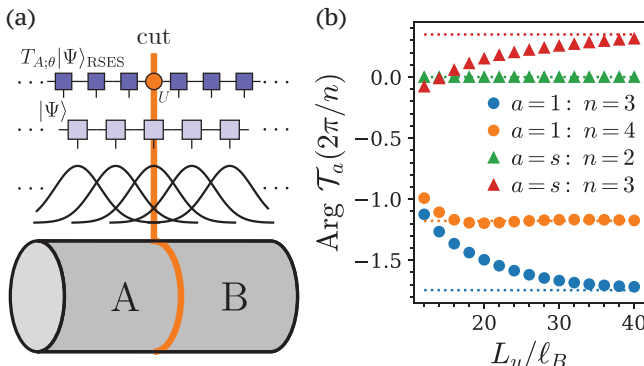


FIG. 3. (a) A schematics of the infinite cylinder geometry and the LLL orbital basis of the MPS. Partial rotation along a real-space cut can be accomplished by acting a unitary operator on the auxiliary bond of the MPS obtained by the RSES algorithm. (b) $\text{Arg} \mathcal{T}_a(2\pi/n)$ of the $\nu = 1/2$ bosonic Laughlin state extracted using Eq. (13). The dotted lines are the CFT predictions given in Table I.

The second example we consider is the $\nu = 1/2$ bosonic Laughlin state, which realizes $U(1)_2$ Chern-Simons theory. Its only non-trivial anyon is the semion s with topological twist $\theta_s = i$.

The model we study is a two-dimensional boson gas projected to the lowest Landau level (LLL) that interacts with a contact interaction $V_0 = 1$ plus a small perturbation $\delta V_2 = 0.1$, where V_m are the Haldane pseudopotentials [21]. The ground state of the system at $\nu = 1/2$ filling is known to be the $\nu = 1/2$ Laughlin state [22]. To compute the partial rotation, we consider an infinite cylinder geometry, as shown in Fig. 3 (a), and use infinite density matrix renormalization group (iDMRG) calculations [23] to obtain the infinite matrix product state (iMPS) representation of the ground state $|\Psi\rangle$.

Compared to other numerical methods, the MPS representation is advantageous for evaluating the action of partial rotation. If rotation is a good symmetry, the Schmidt states $|\alpha\rangle_{A/B}$ across subsystems A and B have definite momentum k_y^α along the circumference. Thus, the action of partial rotation can be evaluated by

$$\mathcal{T}_a(\theta) = \sum_\alpha \lambda_\alpha^2 e^{ik_y^\alpha L_y \theta}, \quad (13)$$

where λ_α is the corresponding Schmidt value. We can easily obtain both k_y^α and λ_α from the momentum label $\bar{K}_{\bar{n}_B; \alpha}$ and the Schmidt value $\lambda_{\bar{n}_B; \alpha}$ of the auxiliary bond \bar{n}_B across subsystems A and B.

For the $\nu = 1/2$ bosonic Laughlin state, we work in the Landau gauge and the corresponding LLL orbital basis. To accelerate the calculation and obtain the momentum label mentioned above, we incorporate both particle number $\hat{C} = \sum_n \hat{C}_n \equiv \sum_n (\hat{N}_n - \nu)$ and momentum $\hat{K} = \sum_n \hat{K}_n \equiv \sum_n n(\hat{N}_n - \nu)$ conservation, where \hat{N}_n is the number operator at site n . We find that $\mathcal{T}_a(2\pi/n)$ converges at bond dimension $\chi = 3200$, cylinder circumference $L_y = 40\ell_B$ and onsite boson number cutoff $N_{\text{boson}} = 5$.

We note there are a few technical complications in applying Eq. (13) to compute $\mathcal{T}_a(\theta)$, which we will scratch here and readers can find more details in Supplemental Materials. First of all, there are a few ambiguities in extracting the physical momentum k_y^α from the momentum label $\bar{K}_{\bar{n}_A; \alpha}$. For iMPS, there is an overall ambiguity of momentum labels on auxiliary bonds. The magnetic translation symmetry in quantum Hall systems further tangles the momentum label $\bar{K}_{\bar{n}; \alpha} = \langle \sum_{n < \bar{n}} \hat{K}_n \rangle_\alpha$ with the charge label $\bar{C}_{\bar{n}; \alpha} = \langle \sum_{n < \bar{n}} \hat{C}_n \rangle_\alpha$ [24]. These ambiguities can be fixed by matching the entanglement spectrum and the edge CFT spectrum as elaborated in Supplemental Materials.

Secondly, which topological sector subsystem A, B belongs to depends on the cut. The $\nu = 1/2$ bosonic Laughlin state has a two-fold ground state degeneracy, characterized by root configuration (pattern of zeros) [01] and [10] [25, 26]. It turns out that cutting through the LLL orbital center that corresponds to the 0's (1's) bisects the system into two trivial sectors (semion) sectors. Finally, when we work in the LLL orbital basis, an auxiliary bond divides the system into two sets of LLL orbitals instead of two regions of physical space. This problem can be resolved using the real-space entanglement spectrum (RSES) algorithm developed in Ref. 24. We note that many of the technicalities discussed here are not specific to the $\nu = 1/2$ bosonic Laughlin state, but provide a general procedure for computing higher central charge of arbitrary wavefunction in the MPS form.

Finally we present the result of $\mathcal{T}_a(2\pi/n)$ in both the trivial and the semion sector. As shown in Fig. 3 (b), $\mathcal{T}_a(2\pi/n)$ always converges to the expected phase as shown in Table I at sufficiently large L_y .

Discussion – In this Letter, we provide a characterization of the higher central charges $\{\zeta_n\}$ in terms of

the partial rotation evaluated on a wavefunction of the (2+1)D bosonic topological order, and confirmed the prediction using the Kitaev honeycomb model and the $\nu = 1/2$ bosonic Laughlin state. Partial rotation can be implemented easily in quantum computing architectures with cheap SWAP gates, such as Rydberg atom arrays, which opens up another avenue to studying topological order directly on a quantum computer.

For future work, it would be interesting to find a way to extract the Frobenius-Schur exponent N_{FS} for a given single wavefunction. Together with the extraction of higher central charge in this Letter, knowing N_{FS} would enable us to completely determine whether the bosonic Abelian topological order has a gappable edge or not. In particular, once we figure out N_{FS} , one can immediately extract chiral central charge from the partial rotation

$$\mathcal{T}_1 \left(\frac{2\pi}{N_{\text{FS}}} \right) \propto e^{-2\pi i \left(\frac{2}{N_{\text{FS}}} + N_{\text{FS}} \right) \frac{c}{24}}, \quad (14)$$

and accordingly all other higher central charges $\{\zeta_n\}$ for $1 < n < N_{\text{FS}}$ by the partial rotations.

Even when we do not know N_{FS} precisely, numerical results of $\{\mathcal{T}_1(2\pi/n)\}$ can put a tight constraint on the possible low-energy spectrum of the bulk-boundary system. For instance, suppose that we observed $\{\mathcal{T}_1(2\pi/p_j)\}$ is a non-trivial phase for a set of distinct prime numbers $\{p_j\}$. One can see that this leaves us two possibilities: 1. the edge is ungappable, or 2. the edge is gappable, where N_{FS} must be divisible by $\prod_j p_j$. If the minimal N_{FS} required for a gappable edge is large and physically unrealistic, one can essentially determine that the boundary must be ungappable.

Remarkably, the lower bound $N_{\text{FS}} \geq \prod_j p_j$ for a gappable edge implies the lower bound for the number of anyons r given by $r \geq r_0$, with r_0 the smallest integer satisfying $2^{2r_0/3+8}3^{2r_0/3} \geq \prod_j p_j$. This can be de-

rived from the fact that N_{FS} of the bosonic topological order with r distinct anyons has the upper bound $N_{\text{FS}} \leq 2^{2r/3+8}3^{2r/3}$ [27]. It implies that the ground state on a torus must carry at least r_0 -fold degeneracy in order to realize a gappable edge. This argument is reminiscent of the Lieb-Schultz-Mattis type theorems [28–30], which constrains the low-energy spectrum for a given input of the symmetry action on the ground state.

Also, it would be interesting to extract the higher version of electric Hall conductivity proposed in Ref. [31], which gives an obstruction to U(1) symmetry-preserving gapped boundary of the fermionic topological order with U(1) symmetry beyond electric Hall conductivity and c_- .

Acknowledgements – We thank Tianle Wang and Mike Zaletel for helpful discussions. RK is supported by the JQI postdoctoral fellowship at the University of Maryland. TW is supported by the U.S. DOE, Office of Science, Office of Basic Energy Sciences, Materials Sciences and Engineering Division, under Contract No. DE-AC02-05-CH11231, within the van der Waals Heterostructures Program (KCWF16). TS is supported by a fellowship from the Masason foundation. RM is supported by the National Science Foundation under Award No. DMR-1848336. SR is supported by the National Science Foundation under Award No. DMR-2001181, and by a Simons Investigator Grant from the Simons Foundation (Award No. 566116). This work is supported by the Gordon and Betty Moore Foundation through Grant GBMF8685 toward the Princeton theory program. This research used the Lawrencium computational cluster resource provided by the IT Division at the Lawrence Berkeley National Laboratory (Supported by the Director, Office of Science, Office of Basic Energy Sciences, of the U.S. Department of Energy under Contract No. DE-AC02-05CH11231).

[1] X.-G. Wen, *Quantum field theory of many-body systems: from the origin of sound to an origin of light and electrons* (Oxford University Press, 2004).

[2] Y. Hatsugai, *Phys. Rev. Lett.* **71**, 3697 (1993).

[3] C. L. Kane and M. P. A. Fisher, *Phys. Rev. B* **55**, 15832 (1997).

[4] I. H. Kim, B. Shi, K. Kato, and V. V. Albert, *Physical Review Letters* **128** (2022), 10.1103/physrevlett.128.176402.

[5] Y. Zou, B. Shi, J. Sorce, I. T. Lim, and I. H. Kim, *Physical Review Letters* **129** (2022), 10.1103/physrevlett.129.260402.

[6] R. Fan, *Physical Review Letters* **129** (2022), 10.1103/physrevlett.129.260403.

[7] R. Fan, R. Sahay, and A. Vishwanath, “Extracting the quantum hall conductance from a single bulk wavefunction,” (2022), arXiv:2208.11710 [cond-mat.str-el].

[8] A. Kapustin and N. Saulina, *Nucl. Phys.* **B845**, 393 (2011), arXiv:1008.0654 [hep-th].

[9] M. Levin, *Physical Review X* **3** (2013), 10.1103/physrevx.3.021009, arXiv:1301.7355 [cond-mat.str-el].

[10] S.-H. Ng, A. Schopieray, and Y. Wang, *Selecta Mathematica* **25** (2019), 10.1007/s00029-019-0499-2, arXiv:1812.11234 [math.QA].

[11] S.-H. Ng, E. C. Rowell, Y. Wang, and Q. Zhang, “Higher central charges and witt groups,” (2020), arXiv:2002.03570 [math.QA].

[12] J. Kaidi, Z. Komargodski, K. Ohmori, S. Seifnashri, and S.-H. Shao, “Higher central charges and topological boundaries in 2+1-dimensional tqfts,” (2021), arXiv:2107.13091 [hep-th].

[13] I. H. Kim, B. Shi, K. Kato, and V. V. Albert, *Physical Review B* **106** (2022), 10.1103/physrevb.106.075147.

[14] A. Kitaev and J. Preskill, *Physical Review Letters* **96** (2006), 10.1103/physrevlett.96.110404, hep-th/0510092.

[15] X.-L. Qi, H. Katsura, and A. W. W. Ludwig, *Physical Review Letters* **108** (2012), 10.1103/physrevlett.108.196402, arXiv:1103.5437 [cond-mat.mes-hall].

[16] H. Li and F. D. M. Haldane, *Phys. Rev. Lett.* **101**, 010504 (2008).

[17] K. Shiozaki, H. Shapourian, and S. Ryu, *Physi-*

cal Review B **95** (2017), 10.1103/physrevb.95.205139, arXiv:1609.05970 [cond-mat.str-el].

[18] H.-H. Tu, Y. Zhang, and X.-L. Qi, Physical Review B **88** (2013), 10.1103/physrevb.88.195412, arXiv:1212.6951.

[19] M. P. Zaletel, R. S. K. Mong, and F. Pollmann, Phys. Rev. Lett. **110**, 236801 (2013).

[20] A. Kitaev, Annals of Physics **321**, 2 (2006), arXiv:cond-mat/0506438.

[21] E. H. Rezayi and F. D. M. Haldane, Phys. Rev. B **50**, 17199 (1994).

[22] B. I. Halperin, J. K. Jain, and N. R. Cooper, “Fractional quantum hall states of bosons: Properties and prospects for experimental realization,” in *Fractional quantum hall effects: New developments* (World Scientific, 2020) p. 487–521.

[23] M. P. Zaletel, R. S. K. Mong, F. Pollmann, and E. H. Rezayi, Phys. Rev. B **91**, 045115 (2015).

[24] M. P. Zaletel and R. S. K. Mong, Phys. Rev. B **86**, 245305 (2012).

[25] B. A. Bernevig and F. D. M. Haldane, Phys. Rev. Lett. **100**, 246802 (2008).

[26] X.-G. Wen and Z. Wang, Phys. Rev. B **78**, 155109 (2008).

[27] P. Bruillard, S.-H. Ng, E. Rowell, and Z. Wang, Journal of the American Mathematical Society **29**, 857 (2015), arXiv:1310.7050.

[28] E. Lieb, T. Schultz, and D. Mattis, Annals of Physics **16**, 407 (1961).

[29] M. Oshikawa, Physical Review Letters **84**, 1535 (2000), arXiv:cond-mat/9911137.

[30] M. Hastings, Physical Review B **69**, 104431 (2004), arXiv:cond-mat/0305505.

[31] R. Kobayashi, Physical Review Research **4** (2022), 10.1103/physrevresearch.4.033137, arXiv:2203.08156.

[32] X.-G. Wen, Phys. Rev. Lett. **90**, 016803 (2003).

[33] S. D. Geraedts, C. Repellin, C. Wang, R. S. K. Mong, T. Senthil, and N. Regnault, Phys. Rev. B **96**, 075148 (2017).

[34] T. Soejima, D. E. Parker, N. Bultinck, J. Hauschild, and M. P. Zaletel, Phys. Rev. B **102**, 205111 (2020).

[35] N. Read, Phys. Rev. B **79**, 045308 (2009).

Supplemental Materials

I. PARTIAL ROTATION OF A CYLINDER IN A TWISTED SECTOR

Here we evaluate the partial rotation in the case where the state lies in the non-trivial topological sector labeled by an anyon a of the topological order. Denoting the ground state as $|\Psi_a\rangle$, the partial rotation is again expressed as the Virasoro characters

$$\begin{aligned} \mathcal{T}_a\left(\frac{2\pi}{n}\right) &= \frac{\text{Tr}_a[e^{iP_l \frac{L}{n}} e^{-\frac{\xi_l}{v} H_l}] \text{Tr}_a[e^{iP_r \frac{L}{n}} e^{-\frac{\xi_r}{v} H_r}]}{\text{Tr}_a[e^{-\frac{\xi_l}{v} H_l}] \text{Tr}_a[e^{-\frac{\xi_r}{v} H_r}]} \\ &= \frac{\chi_a\left(\frac{i\xi_l}{L} + \frac{1}{n}\right) \chi_a\left(\frac{i\xi_r}{L} - \frac{1}{n}\right)}{\chi_a\left(\frac{i\xi_l}{L}\right) \chi_a\left(\frac{i\xi_r}{L}\right)}, \end{aligned} \quad (15)$$

where Tr_a denotes the trace in the twisted Hilbert space labeled by a , and $\chi_a(\tau)$ is the CFT character for the chiral primary a . The above quantity can be evaluated in the same logic as the main text; in our setup where $L \ll \xi_l$, the CFT characters for the left edge are approximated as

$$\begin{aligned} \chi_a\left(\frac{i\xi_l}{L}\right) &\approx e^{-\frac{2\pi\xi_l}{L}(h_a - \frac{c_-}{24})}, \\ \chi_a\left(\frac{i\xi_l}{L} + \frac{1}{n}\right) &\approx e^{-\frac{2\pi\xi_l}{L}(h_a - \frac{c_-}{24})} e^{\frac{2\pi i}{n}(h_a - \frac{c_-}{24})}. \end{aligned} \quad (16)$$

Meanwhile, the characters for the right edge can be approximately computed by performing modular transformations as

$$\chi_a\left(\frac{i\xi_r}{L}\right) = \sum_b S_{ab} \chi_b\left(\frac{iL}{\xi_r}\right) \approx \frac{d_a}{\mathcal{D}} e^{\frac{2\pi L}{\xi_r} \frac{c_-}{24}}, \quad (17)$$

$$\begin{aligned} \chi_a\left(\frac{i\xi_r}{L} - \frac{1}{n}\right) &= \sum_a (ST^n S)_{ab} \chi_b\left(\frac{iL}{n^2 \xi_r} + \frac{1}{n}\right) \\ &\approx (ST^n S)_{a,1} e^{-\frac{2\pi i}{n} \frac{c_-}{24}} e^{\frac{2\pi L}{n^2 \xi_r} \frac{c_-}{24}} \\ &= \frac{1}{\mathcal{D}} e^{-2\pi i(n + \frac{1}{n}) \frac{c_-}{24}} e^{\frac{2\pi L}{n^2 \xi_r} \frac{c_-}{24}} \sum_b S_{ab} d_b \theta_b^n, \end{aligned} \quad (18)$$

where we assumed n to be small, $n^2 \ll L/\xi_r$. Combining the above results, we obtain

$$\mathcal{T}_a\left(\frac{2\pi}{n}\right) \propto e^{\frac{2\pi i}{n}h_a - 2\pi i(\frac{2}{n}+n)\frac{c_-}{24}} \times \sum_b S_{ab} d_b \theta_b^n. \quad (19)$$

II. INTERPOLATING BETWEEN HIGHER CENTRAL CHARGE AND MOMENTUM POLARIZATION

In the main text, we have seen that the partial rotation $\mathcal{T}_1(2\pi/n)$ is proportional to higher central charge for a small positive integer n , while when $n \rightarrow \infty$ it rather gives the momentum polarization λ in Eq. (9). Here, we describe how these two different behaviors are interpolated by changing the value of n from a small integer to infinity. Following Eq. (15) and Eq. (16), we express the partial rotation as

$$\mathcal{T}_a\left(\frac{2\pi}{n}\right) = e^{\frac{2\pi i}{n}(h_a - \frac{c_-}{24})} \times \frac{\chi_a(\frac{i\xi_r}{L} - \frac{1}{n})}{\chi_a(\frac{i\xi_r}{L})}. \quad (20)$$

The Virasoro characters on the right edge is approximated depending on the scale of n compared with L/ξ_r . Below we compute it in cases of the value of n .

- $n^2 \ll L/\xi_r$. The approximation in Eq. (18) is valid for such n and we have

$$\mathcal{T}_a\left(\frac{2\pi}{n}\right) \propto e^{\frac{2\pi i}{n}h_a - 2\pi i(\frac{2}{n}+n)\frac{c_-}{24}} \times \sum_b S_{ab} d_b \theta_b^n. \quad (21)$$

- $L/\xi_r \ll n^2$. When n satisfies $L/\xi_r \ll n^2$, Eq. (18) is no longer valid, where the alternative approximation is available

$$\begin{aligned} \chi_a\left(\frac{i\xi_r}{L} - \frac{1}{n}\right) &= \sum_b S_{ab} \chi_b\left(-\frac{1}{\frac{i\xi_r}{L} - \frac{1}{n}}\right) \\ &\approx \sum_b S_{ab} \exp\left(-2\pi i\left(h_b - \frac{c_-}{24}\right) \frac{1}{\frac{i\xi_r}{L} - \frac{1}{n}}\right) \\ &\approx \frac{d_a}{D} \exp\left(2\pi i \frac{c_-}{24} \frac{1}{\frac{i\xi_r}{L} - \frac{1}{n}}\right). \end{aligned} \quad (22)$$

The partial rotation is then given by

$$\begin{aligned} \mathcal{T}_a\left(\frac{2\pi}{n}\right) &= e^{\frac{2\pi i}{n}(h_a - \frac{c_-}{24})} \exp\left(2\pi i \frac{c_-}{24} \frac{1}{\frac{i\xi_r}{L} - \frac{1}{n}} - \frac{2\pi L}{\xi_r} \frac{c_-}{24}\right) \\ &= \exp\left(\frac{2\pi i}{n}(h_a - \frac{c_-}{24}) - 2\pi i \frac{c_-}{24} \frac{\frac{1}{n}}{\frac{\xi_r^2}{L^2} + \frac{1}{n^2}}\right) \\ &\quad \times \exp\left(2\pi \frac{c_-}{24} \frac{\frac{\xi_r}{L}}{\frac{\xi_r^2}{L^2} + \frac{1}{n^2}} - 2\pi \frac{c_-}{24} \frac{L}{\xi_r}\right). \end{aligned} \quad (23)$$

By taking the limit $n \rightarrow \infty$, it reproduces the expression of momentum polarization in Eq. (9).

III. PREPARING THE TRIVIAL SECTOR OF KITAEV HONEYCOMB MODEL ON A CYLINDER

To compute higher central charge of the topologically ordered state, one needs to prepare a low-energy state on the cylinder that lies in the trivial sector labeled by the trivial anyon 1. In this section, we describe how to obtain such a state for the non-Abelian gapped phase of the Kitaev honeycomb model on a cylinder.

The Kitaev honeycomb model is described in terms of a free fermion model coupled to a dynamical \mathbb{Z}_2 gauge field. The \mathbb{Z}_2 vortex of the gauge field is regarded as a single quasiparticle excitation σ , and the low-energy state is realized by flat \mathbb{Z}_2 gauge field without a vortex on each plaquette. The distinct low-energy states on a cylinder

then correspond to the different configurations of flat \mathbb{Z}_2 gauge field labeled by the boundary conditions of the free fermion model. In particular, the anti-periodic boundary condition (APBC) in the y direction (i.e., circumference) of the cylinder corresponds to 1 or ψ sector, while the periodic (PBC) corresponds to the σ sector. To further obtain the trivial sector 1 instead of ψ , we need to carefully study the holonomy of \mathbb{Z}_2 gauge field in x direction. As we will see below, fixing the holonomy of the \mathbb{Z}_2 gauge field in x direction gives the state labeled by a non-simple anyon $1+\psi$. To obtain a state in the trivial sector 1, it turns out that we need to take a superposition over the two distinct states that correspond to different \mathbb{Z}_2 holonomy in x direction.

Let us move to the explicit description of the states of the Kitaev honeycomb model. We assume that the system size L_y in the y direction is even. Recall that to solve this model, we introduce four Majorana fermion operators b_j^x, b_j^y, b_j^z, c_j on each site j , and the model then becomes equivalent to the free fermion model for the Majorana fermions c , coupled to the dynamical \mathbb{Z}_2 gauge field $u_{ij} := ib_i b_j$ [20]. Let us fix one configuration of flat \mathbb{Z}_2 gauge field of the Kitaev honeycomb model $\{u_{ij}\}$ that corresponds to the APBC in the y direction. For this given configuration of the \mathbb{Z}_2 gauge field $\{u_{ij}\}$, the ground state of the Kitaev honeycomb model is given in the form of

$$|\Psi\rangle = P [|\Psi_F(\{u_{ij}\})\rangle \otimes |\{u_{ij}\}\rangle], \quad (24)$$

where the state is given by the tensor product of the state of the free fermion $|\Psi_F(\{u_{ij}\})\rangle$ and the state $|\{u_{ij}\}\rangle$ for the dynamical \mathbb{Z}_2 field. $P := \prod_j \frac{1+D_j}{2}$ denotes a projection onto the gauge invariant Hilbert space, where $D_j := ib_j^x b_j^y b_j^z c$ generates the gauge transformation at the vertex j .

The distinct state with different \mathbb{Z}_2 holonomy in the x direction can be obtained by considering a straight line l extended in the y direction cutting the links, and then shifting the \mathbb{Z}_2 gauge field $\{u_{ij}\}$ along the links cut by the line l . Let us denote the shifted \mathbb{Z}_2 gauge field as $\{u'_{ij}\}$, and the corresponding state of the Kitaev honeycomb model as

$$|\Psi'\rangle = P [|\Psi_F(\{u'_{ij}\})\rangle \otimes |\{u'_{ij}\}\rangle]. \quad (25)$$

We aim to show that the two states $|\Psi\rangle \pm |\Psi'\rangle$ correspond to the states in the sector 1 and ψ , though we do not try to specify which of $|\Psi\rangle \pm |\Psi'\rangle$ corresponds to the trivial sector. To see this, we evaluate the partial rotation for the states $|\Psi\rangle \pm |\Psi'\rangle$, since the partial rotation can diagnose the distinct topological sector.

To perform the partial rotation, we need to take the bipartition of the cylinder into A and B subsystems. For convenience, let us perform the bipartition along the line l that we used for shifting the \mathbb{Z}_2 gauge field from $\{u_{ij}\}$ to $\{u'_{ij}\}$. Without loss of generality, we can take the gauge where $u_{ij} = 1$ on each link cut by the line l , while $u'_{ij} = -1$ on these links.

Since the link variables u_{ij}, u'_{ij} cut by the line l overlaps the Hilbert space of A and B subsystems, it is convenient to redefine link variables near the cut so that the newly defined ones lie solely in the A or B subsystem. This can be done by following the argument in Appendix A of Ref. [18]. We recall that the link variable is given by the doublet of Majorana fermions as $u_{ij} = ib_i b_j$, and let us write the Majorana fermions at the plaquette on the cut as b_1, b_2, b_3, b_4 as shown in Fig. 4. The newly defined link variables are then given by $w_{13} := ib_1 b_3, w_{42} = ib_4 b_2$. The local Hilbert space spanned by these four Majorana fermions is identified as the Hilbert space of two qubits, where we have the identification of operators as

$$u_{12} = Z_1, \quad u_{34} = Z_2, \quad w_{13} = X_1 X_2, \quad w_{42} = -Y_1 Y_2. \quad (26)$$

Some of the eigenstates of w_{13}, w_{42} are expressed as

$$|++\rangle = \frac{1}{\sqrt{2}}(|00\rangle + |11\rangle), \quad |--\rangle = \frac{1}{\sqrt{2}}(|00\rangle - |11\rangle) \quad (27)$$

where $+, -$ denotes eigenvalues of w_{13}, w_{42} , while $0, 1$ denotes those of u_{12}, u_{34} .

Noting that $u_{ij} = 1$ on the edges cut by the bipartition, the state for the \mathbb{Z}_2 gauge field $|\{u_{ij}\}\rangle$ is decomposed into the Hilbert spaces of A, B subsystems as

$$|\{u_{ij}\}\rangle = 2^{-\frac{L_y}{4}} \sum_{w_{ij}=\pm 1} |\{u_{ij}^A, w_{ij}\}\rangle_A \otimes |\{u_{ij}^B, w_{ij}\}\rangle_B. \quad (28)$$

Meanwhile, since $u'_{ij} = -1$ on the edges cut by the bipartition, the state for the shifted \mathbb{Z}_2 gauge field $|\{u'_{ij}\}\rangle$ is decomposed as

$$|\{u'_{ij}\}\rangle = 2^{-\frac{L_y}{4}} \sum_{w_{ij}=\pm 1} (-1)^{|w|} |\{u_{ij}^A, w_{ij}\}\rangle_A \otimes |\{u_{ij}^B, w_{ij}\}\rangle_B, \quad (29)$$

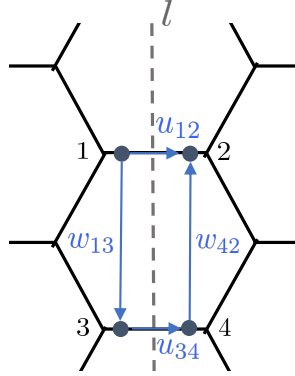


FIG. 4. The link variables near the bipartition. The thick dots denote the Majorana fermions b_j for $1 \leq j \leq 4$. The link variables $u_{12} = ib_1b_2, u_{34} = ib_3b_4$ are cut by the line l , and we define the new ones $w_{13} = ib_1b_3, w_{42} = ib_4b_2$.

where $|w|$ is the mod 2 number of links on the A subsystem with $w_{ij} = -1$. Note that $u_{ij} = u'_{ij}$ away from the cut, so each Schmidt state in the A, B subsystems are the same in the expression of $|\{u_{ij}\}\rangle$ and $|\{u'_{ij}\}\rangle$.

Let us also write the Schmidt decomposition of the free fermion state $|\Psi_F(\{u_{ij}\})\rangle$ as

$$|\Psi_F(\{u_{ij}\})\rangle = \sum_N \alpha_N |\Psi_N^A(\{u_{ij}^A\})\rangle \otimes |\Psi_N^B(\{u_{ij}^B\})\rangle. \quad (30)$$

Next, we assume that the low-energy state for the free fermion $|\Psi_F(\{u'_{ij}\})\rangle$ under the shifted \mathbb{Z}_2 gauge field $\{u'_{ij}\}$ can be chosen to be identical to that under the trivial \mathbb{Z}_2 gauge field $\{u_{ij}\}$,

$$|\Psi_F(\{u'_{ij}\})\rangle = |\Psi_F(\{u_{ij}\})\rangle, \quad (31)$$

and hence has the same Schmidt decomposition. Below, we show that $|\Psi\rangle \pm |\Psi'\rangle$ with the above $|\Psi'\rangle$ corresponds to the 1 or ψ sector.

The reduced density matrix of $|\Psi\rangle$ for the A subsystem is given by [18]

$$\rho_A := \text{Tr}_B(|\Psi\rangle\langle\Psi|) \propto \sum_{w_{ij}=\pm 1} \sum_N |\alpha_N|^2 P_A [|\Psi_N^A(\{u_{ij}^A\})\rangle |\{u_{ij}^A, w_{ij}\}\rangle] P_A [\langle\Psi_N^A(\{u_{ij}^A\})| \langle\{u_{ij}^A, w_{ij}\}|], \quad (32)$$

where $P_A = \prod_{j \in A} \frac{1+D_j}{2}$ denotes the projector supported on the A subsystem. Noting that the product of gauge transformations in the A subsystem $\prod_{j \in A} D_j$ leaves the link variables $\{u_{ij}^A, w_{ij}\}$ invariant, one can rewrite the expression of the state as

$$P_A [|\Psi_N^A(\{u_{ij}^A\})\rangle |\{u_{ij}^A, w_{ij}\}\rangle] \propto \sum_{\{u'_{ij}^A, w'_{ij}\} \approx \{u_{ij}^A, w_{ij}\}} \frac{1 + \prod_{j \in A} D_j}{2} |\Psi_N^A(\{u'_{ij}^A\})\rangle |\{u'_{ij}^A, w'_{ij}\}\rangle \quad (33)$$

where the sum is taken over gauge fields $\{u'_{ij}^A, w'_{ij}\}$ that are equivalent to $\{u_{ij}^A, w_{ij}\}$ up to gauge transformations. The reduced density matrix is then expressed as

$$\rho_{A,|\Psi\rangle} \propto \sum_{w_{ij}=\pm 1} \sum_{\{u'_{ij}^A, w'_{ij}\} \approx \{u_{ij}^A, w_{ij}\}} \sum_N |\alpha_N|^2 \frac{1 + \prod_{j \in A} D_j}{2} |\Psi_N^A(\{u'_{ij}^A\})\rangle |\{u'_{ij}^A, w'_{ij}\}\rangle \langle\Psi_N^A(\{u''_{ij}^A\})| \langle\{u''_{ij}^A, w''_{ij}\}| \frac{1 + \prod_{j \in A} D_j}{2} \quad (34)$$

Also, the reduced density matrix for the state $|\Psi\rangle \pm |\Psi'\rangle$ is given by

$$\begin{aligned} \rho_{A,|\Psi\rangle \pm |\Psi'\rangle} &\propto \sum_{w_{ij}=\pm 1} \frac{1 \pm (-1)^{|w|}}{2} \sum_{\{u'_{ij}^A, w'_{ij}\} \approx \{u_{ij}^A, w_{ij}\}} \sum_N |\alpha_N|^2 \frac{1 + \prod_{j \in A} D_j}{2} |\Psi_N^A(\{u'_{ij}^A\})\rangle |\{u'_{ij}^A, w'_{ij}\}\rangle \langle\Psi_N^A(\{u''_{ij}^A\})| \langle\{u''_{ij}^A, w''_{ij}\}| \frac{1 + \prod_{j \in A} D_j}{2} \\ &= |\alpha_N|^2 \frac{1 + \prod_{j \in A} D_j}{2} |\Psi_N^A(\{u'_{ij}^A\})\rangle |\{u'_{ij}^A, w'_{ij}\}\rangle \langle\Psi_N^A(\{u''_{ij}^A\})| \langle\{u''_{ij}^A, w''_{ij}\}| \frac{1 + \prod_{j \in A} D_j}{2}. \end{aligned} \quad (35)$$

The partial rotation of these reduced density matrices for $|\Psi\rangle, |\Psi\rangle \pm |\Psi'\rangle$ are evaluated as

$$\begin{aligned}\mathcal{T}_{|\Psi\rangle}\left(\frac{2\pi}{n}\right) &\propto \sum_{w_{ij}=\pm 1} \sum_N |\alpha_N|^2 \left\langle \Psi_N^A(\{T_{\frac{L_y}{n}} u_{ij}^A\}) \right| \frac{1 + \prod_{j \in A} D_j}{2} T_{A; \frac{L_y}{n}} \left| \Psi_N^A(\{u_{ij}^A\}) \right\rangle, \\ \mathcal{T}_{|\Psi\rangle \pm |\Psi'\rangle}\left(\frac{2\pi}{n}\right) &\propto \sum_{w_{ij}=\pm 1} \sum_N |\alpha_N|^2 \left\langle \Psi_N^A(\{T_{\frac{L_y}{n}} u_{ij}^A\}) \right| \frac{1 \pm (-1)^{|w|}}{2} \frac{1 + \prod_{j \in A} D_j}{2} T_{A; \frac{L_y}{n}} \left| \Psi_N^A(\{u_{ij}^A\}) \right\rangle,\end{aligned}\quad (36)$$

where we assume L_y is the integer multiple of n , and $T_{A; \frac{L_y}{n}}$ is the translation along the y direction by L_y/n lattice units. $\{T_{\frac{L_y}{n}} u_{ij}^A\}$ denotes the gauge field obtained by acting the translation $T_{A; \frac{L_y}{n}}$ on the configuration $\{u_{ij}\}$. The above expressions for the partial rotation can further be simplified by writing the operator $\prod_{j \in A} D_j$ as

$$\prod_{j \in A} D_j = (-1)^F (-1)^{|w|} \prod_{j \in A} u_{ij}^A, \quad (37)$$

where $(-1)^F$ is the fermion parity operator of the A subsystem acting only on the free fermion state. The product over link variables are dependent on the orientations of the links, but its detailed definition is not discussed here. Since the projector $\frac{1 + \prod_{j \in A} D_j}{2}$ enforces the relation $(-1)^F = (-1)^{|w|} \prod_{j \in A} u_{ij}^A$ and we sum over all possible choices of $w_{ij} = \pm 1$, the half of the projectors in the summand of w_{ij} becomes $\frac{1 + (-1)^F}{2}$, while the other half becomes $\frac{1 - (-1)^F}{2}$. Hence we have

$$\sum_{w_{ij}=\pm 1} \frac{1 + \prod_{j \in A} D_j}{2} \propto \frac{1 + (-1)^F}{2} + \frac{1 - (-1)^F}{2} = 1. \quad (38)$$

Meanwhile, for the operator $\frac{1 \pm (-1)^{|w|}}{2} \frac{1 + \prod_{j \in A} D_j}{2}$, the contribution of either $\frac{1 + (-1)^F}{2}$ or $\frac{1 - (-1)^F}{2}$ is suppressed by the presence of the $\frac{1 \pm (-1)^{|w|}}{2}$ factor. We hence have

$$\sum_{w_{ij}=\pm 1} \frac{1 \pm (-1)^{|w|}}{2} \frac{1 + \prod_{j \in A} D_j}{2} \propto \frac{1 + (-1)^F}{2} \quad \text{or} \quad \frac{1 - (-1)^F}{2}. \quad (39)$$

Eventually, one can express the partial rotation of each state in the form only involving the free fermion state as

$$\mathcal{T}_{|\Psi\rangle}\left(\frac{2\pi}{n}\right) \propto \sum_N |\alpha_N|^2 \left\langle \Psi_N^A(\{T_{\frac{L_y}{n}} u_{ij}^A\}) \right| T_{A; \frac{L_y}{n}} \left| \Psi_N^A(\{u_{ij}^A\}) \right\rangle, \quad (40)$$

$$\mathcal{T}_{|\Psi\rangle \pm |\Psi'\rangle}\left(\frac{2\pi}{n}\right) \propto \begin{cases} \sum_N |\alpha_N|^2 \left\langle \Psi_N^A(\{T_{\frac{L_y}{n}} u_{ij}^A\}) \right| \frac{1 + (-1)^F}{2} T_{A; \frac{L_y}{n}} \left| \Psi_N^A(\{u_{ij}^A\}) \right\rangle, \\ \text{or} \\ \sum_N |\alpha_N|^2 \left\langle \Psi_N^A(\{T_{\frac{L_y}{n}} u_{ij}^A\}) \right| \frac{1 - (-1)^F}{2} T_{A; \frac{L_y}{n}} \left| \Psi_N^A(\{u_{ij}^A\}) \right\rangle. \end{cases} \quad (41)$$

Let us write the entanglement Hamiltonian of the free fermion state $|\Psi_F(\{u_{ij}^A\})\rangle$ as H_E . The above partial rotations are then simply expressed as

$$\mathcal{T}_{|\Psi\rangle}\left(\frac{2\pi}{n}\right) \propto \text{Tr} \left(e^{-H_E} T_{A; \frac{L_y}{n}} \right), \quad (42)$$

$$\mathcal{T}_{|\Psi\rangle \pm |\Psi'\rangle}\left(\frac{2\pi}{n}\right) \propto \text{Tr} \left(\frac{1 + (-1)^F}{2} e^{-H_E} T_{A; \frac{L_y}{n}} \right) \quad \text{or} \quad \text{Tr} \left(\frac{1 - (-1)^F}{2} e^{-H_E} T_{A; \frac{L_y}{n}} \right). \quad (43)$$

At the CFT level, the projector $(1 + (-1)^F)/2$ (resp. $(1 - (-1)^F)/2$) corresponds to the projector onto the fermion parity even (resp. odd) Hilbert space, which corresponds to the sector 1 (resp. ψ). We hence have

$$\mathcal{T}_1\left(\frac{2\pi}{n}\right) \propto \text{Tr} \left(\frac{1 + (-1)^F}{2} e^{-H_E} T_{A; \frac{L_y}{n}} \right), \quad \mathcal{T}_\psi\left(\frac{2\pi}{n}\right) \propto \text{Tr} \left(\frac{1 - (-1)^F}{2} e^{-H_E} T_{A; \frac{L_y}{n}} \right). \quad (44)$$

In the main text, we directly confirm the first relation for $\mathcal{T}_1\left(\frac{2\pi}{n}\right)$ by comparing the CFT results for LHS and the numerical results for RHS.

IV. EXTRACTING HIGHER CENTRAL CHARGE OF THE KITAEV HONEYCOMB MODEL

The Kitaev honeycomb model supports two types of topological orders [20]: the toric code phase with $c_- = 0$ and the Ising topological order with $c_- = 1/2$. In this appendix, we show the higher central charges of these two phases, and see how they interpolate at finite L_y .

The toric code phase is obtained when one of J_x, J_y, J_z is much larger than other e.g. $|J_x| > |J_y| + |J_z|$. Perturbation theory calculation confirms the effective theory for this corresponds to Wen's plaquette model [32]. Let us now consider the phase with $|J_z| > |J_y| + |J_x|$. With the zigzag boundary condition given in Fig. 2, this corresponds to a edge critical theory between the m and e type boundaries. However, since all topological sectors of toric code has trivial $\zeta_{n,a}$, this does not affect the extraction of partial rotation. Therefore, we will simply reuse the formula Eq.(12) and its σ phase counterpart to compute partial rotation, even though it no longer corresponds to the trivial or σ sector of the Ising topological order.

In Fig. 5(a)-(d), we show the convergence of higher central charge with circumference L_y , both for the toric code phase and the Ising phase. The toric code phase has four Abelian anyons with topological spins $\theta_1 = 1, \theta_m = 1, \theta_e = 1, \theta_f = -1$, and correspondingly the higher central charge is always real and positive. We see ζ_n converges quickly to their theoretical values. In Fig. 5 (e), we show the partial rotation $\mathcal{T}_a(2\pi/n)$. At this fixed L_y , phase angle smoothly interpolates between the Ising phase and the toric code phase.

V. EVALUATING THE ACTION OF PARTIAL ROTATION OF AN MPS WAVE FUNCTION

Here we explain how to evaluate the action of partial rotation of an MPS wave function, with quantum Hall systems as an example. In the following we will first review the quantum Hall DMRG setup developed in Ref. 19, 24, and 33. We consider an infinite cylinder geometry with y running around the circumference, and x running along the infinite direction (see Fig. 1). We work in the Landau gauge and the corresponding LLL orbital takes the form (see Fig. 3 (a))

$$\varphi_n(x, y) = \frac{e^{ik_n y - \frac{1}{2\ell_B^2} (x - k_y^n \ell_B^2)^2}}{\sqrt{L_y \ell_B \pi^{1/2}}}, \quad k_y^n = \frac{2\pi n}{L_y} \quad (45)$$

where $n \in \mathbb{Z}$ and orbital n localizes at $k_n \ell_B^2 = 2\pi n \ell_B / L_y$. We note that in order to perform the partial rotation, it is important to work in an eigenbasis in momentum k_y , which implicitly assumes translation symmetry, continuous or discrete, along the y direction. For a lattice model or a k -space continuum model, such a basis can be obtained by hybrid Wannier localization in the y direction, which maps the original model to a cylinder in mixed (x, k_y) basis [34].

There is a natural one-dimensional iMPS representation of quantum Hall wavefunction in this basis,

$$|\Psi[B]\rangle = \sum_{\{j_n\}} \left[\dots B^{[0]j_0} B^{[1]j_1} \dots \right] | \dots, j_0, j_1, \dots \rangle \quad (46)$$

where $B^{[n]j_n}$ are $\chi \times \chi$ matrices and $|j_n\rangle, j_n \in \{0, 1, \dots, N_{\text{boson}}\}$ represent the boson occupancy at orbital n . Both bond dimension χ and onsite boson number cutoff N_{boson} constrain the representability of the iMPS. However, as we will show in later sections of the Supplemental Materials, the partial rotation $\mathcal{T}_a(2\pi/n)$ quickly saturates to its true value at relatively small χ and N_{boson} .

One key ingredient to accelerate the DMRG algorithm and allow the action of partial rotation is to implement both particle number and momentum conservation,

$$\hat{C} = \sum_n \hat{C}_n \equiv \sum_n \left(\hat{N}_n - \frac{p}{q} \right), \quad \hat{K} = \sum_n \hat{K}_n \equiv \sum_n n \left(\hat{N}_n - \frac{p}{q} \right) \quad (47)$$

where \hat{N}_n is the number operator at site n and $\nu = p/q$. Now for a generic U(1) charge conservation $\hat{Q} = \hat{C}/\hat{K}$, we can decompose the symmetry operator \hat{Q} into $\hat{Q} = \sum_{n < \bar{n}} \hat{Q}_n + \sum_{n > \bar{n}} \hat{Q}_n = \hat{Q}_A + \hat{Q}_B$, where \bar{n} is the auxiliary bond across A and B. For the moment we will assume A, B represent two sets of LLL orbitals and discuss the difference between orbital-space cut and real-space cut later. Then for a Schmidt decomposition across bond \bar{n} , $|\Psi\rangle = \sum_\alpha \lambda_\alpha^2 |\alpha\rangle_A \otimes |\alpha\rangle_B$, we can require the Schmidt states to be eigenstates of $\hat{Q}_{A/B}$,

$$\hat{Q}_B |\alpha\rangle_B = \bar{Q}_{\bar{n};\alpha} |\alpha\rangle_B \quad (48)$$

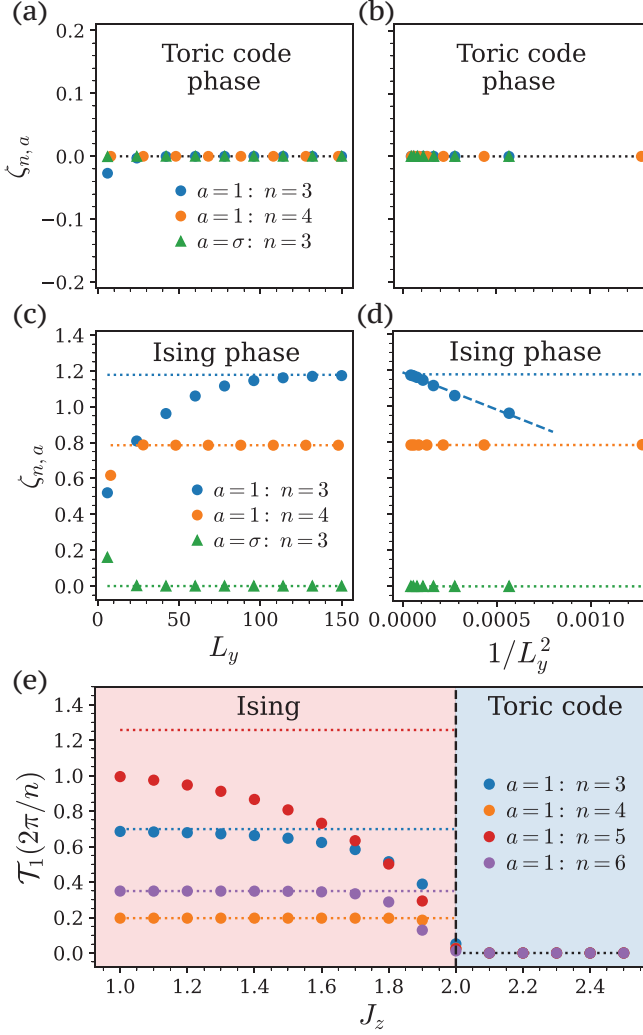


FIG. 5. (a) Higher central charge ζ_n of the toric code phase of the Kitaev model, extracted from $\mathcal{T}_a(2\pi/n)$ in Fig. 2 (b) and chiral central charge $c_- = 0$ using the main result Eq. (2), computed using $J_x = 2.5, J_y = J_z = 1, \kappa = 0$. The dotted lines are the CFT predictions as usual. (b) Extrapolating ζ_n as a function of $1/L_y^2$ (c) Twisted higher central charge $\zeta_{n,a}$ of the Ising phase of the Kitaev model, extracted using chiral central charge $c_- = 1/2$. The computation is done with $J_x = J_y = J_z = 1, \kappa = 0.1$. (d) Extrapolating $\zeta_{n,a}$ as a function of $1/L_y^2$. (e) Phase of partial rotation $\mathcal{T}_1(2\pi/n)$ as it goes through a phase transition from the Ising phase to the toric code phase. $J_z = 2$ line marks the phase transition, and the horizontal dashed (dotted) lines are CFT predictions for Ising (toric code) phase. The computation is done with $J_x = J_y = 1, \kappa = 0.1, L_x = 100, L_y = 120$.

At the level of MPS, local charge conservation on site n takes the form,

$$\left[\bar{Q}_{\bar{n};\beta} - \bar{Q}_{\bar{n}+1;\alpha} - \hat{Q}_{n;j} \right] B_{\alpha\beta}^{[n]j} = 0 \quad (49)$$

where $\bar{n} < n < \bar{n} + 1$. This conservation law naturally generalizes to the corresponding symmetry action. For example, pictorially, momentum conservation means pictorially means

Diagram (50) shows the symmetry action of rotating site n along the y direction by angle θ . The left side shows a blue square and a red circle connected by a line, with a label $e^{i\theta\hat{K}_n}$ below it. The right side shows a red circle, a blue square, and a red circle connected by lines, with labels $e^{-i\theta\hat{K}_{\bar{n}}}$ and $e^{i\theta\hat{K}_{\bar{n}+1}}$ below them. The two sides are connected by an equals sign.

where $\hat{U} = e^{i\theta\hat{K}}$ is the symmetry action of rotating site n along the y direction by angle θ .

A. Partial rotate an MPS

Now we explain how to exploit the implemented momentum conservation to perform the partial rotation. Naively, $\hat{K}_B = \sum_{n>\bar{n}} \hat{K}_n$ has the interpretation of total momentum to the right of bond \bar{n} , so one would expect the action of partial rotation of angle θ to be

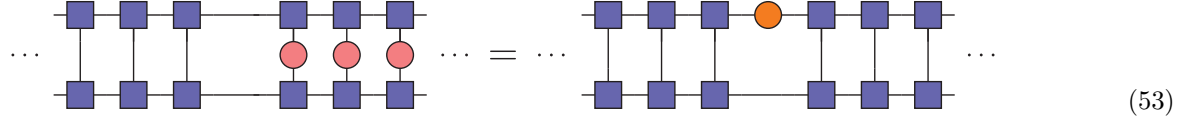
$$e^{-i\theta\hat{K}_B} |\Psi\rangle = e^{-i\theta\hat{K}_B} \sum_{\alpha} \lambda_{\alpha} |\alpha\rangle_A \otimes |\alpha\rangle_B = \sum_{\alpha} \lambda_{\alpha}^2 e^{-i\theta\bar{K}_{\bar{n};\alpha}} |\alpha\rangle_A \otimes |\alpha\rangle_B \quad (51)$$

This would be obvious for a finite MPS whose momentum eigenvalues $\bar{K}_{\bar{n};\alpha}$ are finite. However, for iMPS, a more rigorous proof presented below would be appreciated.

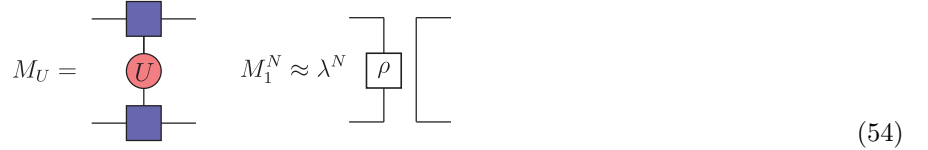
Theorem 1. For an infinite MPS $|\Psi\rangle$, the expectation value $\mathcal{T}_a(\theta)$ of partial rotating all sites in B by angle θ is equivalent to inserting a $e^{-i\theta\bar{K}_{\bar{n};\alpha}}$ factor to the bond \bar{n} across A, B.

$$\langle \Psi | \prod_{n>\bar{n}} e^{i\theta\hat{K}_n} |\Psi\rangle = \sum_{\alpha} \lambda_{\alpha}^2 \langle \alpha|_A \otimes \langle \alpha|_B e^{-i\theta\bar{K}_{\bar{n};\alpha}} |\alpha\rangle_A \otimes |\alpha\rangle_B = \sum_{\alpha} \lambda_{\alpha}^2 e^{-i\theta\bar{K}_{\bar{n};\alpha}} \quad (52)$$

Pictorially,



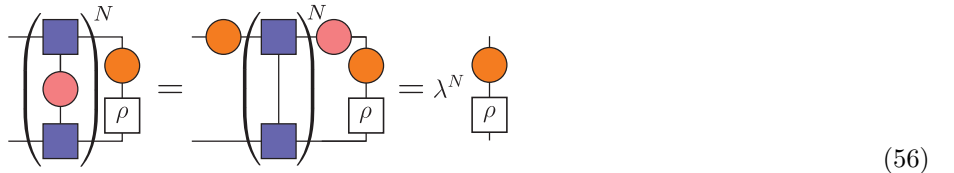
Proof. To prove this theorem, we introduce the formulation of transfer matrices. For simplicity, we assume the unit cell size to be one in the following proof. The transfer matrix M_U is defined to be $M_U = \sum_{j,j'} U_{j,j'} B^j \otimes B^{j'}$. The most important property of transfer matrix M_1 (with no operator insertion) is that we can approximate M_1^N by its dominant eigenvector ρ with eigenvalue $\lambda = 1$,



since all eigenvectors with eigenvalue $\lambda' < 1$ would be negligible in the iMPS limit $N \rightarrow \infty$. The theorem can be rewritten in a more precise form using the language of transfer matrices,

$$M_U^N \approx e^{i\phi} \bar{U}^{-1} M_1^N, \quad \text{where } U = e^{i\theta\hat{K}_n}, \quad \bar{U}^{-1} = e^{-i\theta\bar{K}_{\bar{n};\alpha}} \rho_{\alpha,\alpha'} \quad (55)$$

where ϕ is an overall phase ambiguity. Using the momentum conservation in Eq. (49), we can show $e^{-i\theta\bar{K}_{\bar{n};\alpha}} \rho_{\alpha,\alpha'}$ is an eigenvector of M_U with eigenvalue $\lambda = 1$, which therefore must be the dominant eigenvector of M_U ,



We note that $e^{i\phi} e^{-i\theta\bar{K}_{\bar{n};\alpha}} \rho_{\alpha,\alpha'}$ is also a dominant eigenvector, so there is an overall phase ambiguity that cannot be determined by this argument. We will see the consequence of this ambiguity in the next section. Combined with the property of transfer matrix in Eq. (54), we have established $M_U^N \approx e^{i\phi} \bar{U}^{-1} M_1^N$ and therefore proved the theorem. \square

B. Matching iMPS momentum labels to CFT momentums

The most subtle but important aspect in the evaluation of partial rotation is to resolve some of the gauge freedoms in matching the momentum labels \bar{K}_{α} in the iMPS representation to the CFT momentum labels of a state. The

conserved-charges (i.e., charge and momentum) labels for particles on each site are given by Eq. (47). The conserved-charge labels for the Schmidt states across any bond is the accumulations of the those to the left of the cut; which is sensitive even to electrons and dipole that are far away from the entanglement cut. As we “grow” the MPS chain in the iDMRG algorithm, such electrons/dipoles may be “stuck” based on the initialization of the DMRG. For example, an electron far away may shift the conserved-charge labels via $\hat{C} \rightarrow \hat{C} + q$ and $\hat{K} \rightarrow \hat{K} + d_{\text{electron}}\hat{C}$, where d_{electron} is the distance (proportional to number of DMRG steps) of the charge. Therefore the momentum label $\bar{K}_{\bar{n};\alpha}$ has two integer ambiguity x_0 and x_1 to be determined,

$$\bar{K}_\alpha \mapsto \bar{K}'_\alpha = \bar{K}_\alpha + x_1 \bar{C}_\alpha + x_0. \quad (57)$$

To reproduce the CFT calculation in Eq. (2), we can match the entanglement spectrum and the (1+1)D edge CFT spectrum to fix the momentum labels. We demand, for the ground state corresponding to the vacuum, that (a) the highest weight state (corresponding to the lowest energy state of the entanglement Hamiltonian) has zero momentum and charge, and (b) that sectors with opposite charges have the same momentum labels. (For the semion ground state, its entanglement spectrum has two highest weight state—we assign them to have charges $\pm 1/2$ and zero momentum.)

C. Orbital cut v.s. real-space cut

Now we are ready to talk about the difference between the orbital cut and real-space cut. The CFT prediction in Eq. (2) assumes a real space partition. Before we explain the numerical realization, we first discuss the physical implication of a real-space cut at different locations. In quantum Hall systems, the entanglement spectrum depends on the where the real-space cut is made. In particular, we want to make the cut such that anyon a can appear right on the cut, then the entanglement spectrum would agree best with the 1D edge CFT spectrum. For fermions, this happens when the cut is in the middle of two LLL orbital centers; for bosons, this happens when the cut is right at the LLL orbital center.

This is most obvious in the thin cylinder limit, where the $\nu = 1/2$ bosonic Laughlin state takes the form of

$$|\Psi\rangle = |\cdots 010101 \cdots\rangle \quad (58)$$

in the occupation basis. This is usually referred as the root configuration of the state (or pattern of zeros). For the entanglement spectrum corresponding to the vacuum sector, we want to choose the boundaries of the unit cell such that the electron (i.e., the ‘1’ of the root configuration) is in the middle of the unit cell. (This ensures that entanglement spectrum has a unique highest weight state and a symmetry between positive and negative charge selection sectors.) The real-space cut corresponding to boundaries of the unit cell.

Therefore, cutting through the 0’s gives the trivial sector and cutting through the 1’s (related by threading one flux quanta through the cylinder) gives the semion sector. Furthermore, this also explains why for fermionic Laughlin states (q odd), the unit cell cuts between a pair of neighboring sites. This identification remains true at finite circumference L .

Finally, we briefly explain the numerical realization of the real-space cut. We take the most straightforward approach based on the real-space entanglement spectrum (RSES) algorithm developed in Ref. 24. For a real-space partition at $x = x_c$, RSES algorithm reconstructs the orbital space MPS $|\Psi[B]\rangle$ obtained in iDMRG into a new one $|\psi[B]_{\text{RSES}}\rangle$ such that a particular bond \bar{n}_c gives the real-space Schmidt decomposition at x_c . This is accomplished by splitting each matrix $B^{[n]}$ into two $B_A^{[n]}$ and $B_B^{[n]}$ based on the weight of the orbital φ_n supported on A, B, and then swap all $B_A^{[n]}$ to the left of bond \bar{n}_c and $B_B^{[n]}$ to the right. Then we can easily evaluate the action of partial rotation with the techniques discussed above. We note that the difference between orbital cut and real-space cut is quite general in systems where band projection was used, since the Wannier function usually span across a few sites.

VI. EXTRACTING HIGHER CENTRAL CHARGE OF THE $\nu = 1/2$ BOSONIC LAUGHLIN STATE

A. Extracting higher central charge from scratch

In the main text Fig. 3, we only present the numerical result of $\mathcal{T}_a(2\pi/n)$. We note that $\mathcal{T}_a(2\pi/n)$ itself is sufficient in determining the gappability of the edge, without referring to the actual value of the higher central charge ζ_n . However, if one wants to extract ζ_n , one also needs to know about the chiral central charge c_- , which could be obtained from either some prior knowledge about the topological order, or the momentum polarization [18, 19], or certain entanglement measures [4, 6, 7, 13]. Our numerical algorithm can easily reproduce the momentum polarization by taking the large n limit, though the physics is completely different as explained in the main text. For completeness, we show the momentum polarization, and the resulting higher central charge in this section.

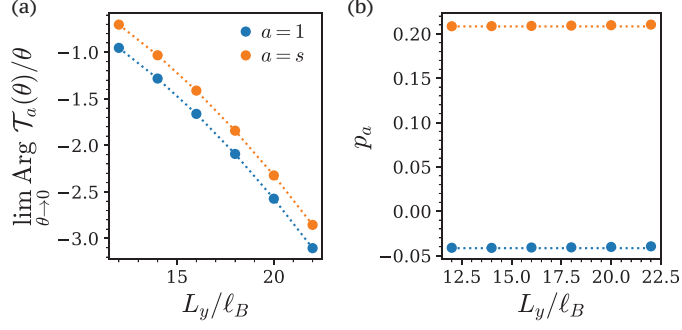


FIG. 6. (a) Infinitesimal rotation $\lim_{\theta \rightarrow 0} \text{Arg } \mathcal{T}_a(2\pi/n)$ of the $\nu = 1/2$ bosonic Laughlin state extracted using Eq. (13). (b) The corresponding momentum polarization $p_a = h_a - c_-/24$ extracted using Eq. (9). The dotted lines are the CFT predictions.

In quantum Hall systems, the momentum polarization takes the universal form [19]

$$\lim_{n \rightarrow \infty} \mathcal{T}_a \left(\frac{2\pi}{n} \right) = \exp \left[\frac{2\pi i}{n} \left(h_a - \frac{c_-}{24} - \frac{\eta_H}{2\pi\hbar} L^2 \right) \right] \quad (59)$$

where $\eta_H = \hbar\nu\mathcal{S}/8\pi\ell_B^2$ is the universal Hall viscosity with \mathcal{S} being the topological shift [35]. We first evaluate the action of infinitesimal rotation and then fit the result to Eq. (59) (see Fig. 6 (a)), where we find $\mathcal{S} = 1.998$ for both topological sectors, in excellent agreement of the CFT prediction $\mathcal{S} = 2$. Subtracting off the the Hall viscosity contribution, we plot the resulting momentum polarization $p_a = h_a - c_-/24$ in Fig. 6 (b), which again gives the expected $c_- = 1$ and $h_s = 1/4$. We note that we can only reach $L_y = 22\ell_B$ using the largest practical onsite boson cutoff N_{boson} , whereas for partial rotation we can easily reach $L_y > 40\ell_B$. This is because a much higher precision is required in evaluating $\mathcal{T}_a(2\pi/n)$ in order to reliable extract p_a , a point we will return to in the next section.

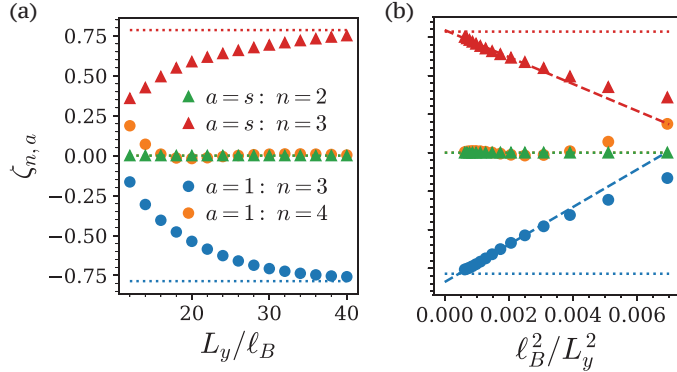


FIG. 7. (a) (Twisted) higher central charge $\zeta_{n,a}$ extracted from $\mathcal{T}_a(2\pi/n)$ in Fig. 3 (b) and chiral central charge $c_- = 1$ in Fig. 6 using the main result Eq. (2). The dotted lines are the CFT predictions as usual. (b) Extrapolating $\zeta_{n,a}$ as a function of ℓ_B^2/L_y^2 .

Using $c_- = 1$ and $h_s = 1/4$ extracted from momentum polarization, we can extract the (twisted) higher central charge $\zeta_{n,a}$ using the main result Eq. (2). As shown in Fig. 7, $\zeta_{n,a}$ all converge to the expected values as shown in Table I at sufficiently large L_y .

B. Numerical performance of partial rotation

Now we briefly discuss the numerical performance of our protocol to extract higher central charge from partial rotating an MPS wavefunction. Compared to free fermion models, e.g. the Kitaev model, the MPS representation of a topological state wavefunction is generically not exact. Both the bond dimension χ and the onsite boson number cutoff N_{Boson} put constraints on the representability of the MPS. However, the quantity we are interested in, i.e. the partial rotation $\mathcal{T}_a(2\pi/n)$ rapidly saturates to its true value up to the largest system size we reach (see Fig. 8). In practice, for a relatively small χ and N_{Boson} , we can already obtain $\mathcal{T}_a(2\pi/n)$ and therefore $\zeta_{n,a}$ to rather high precision.

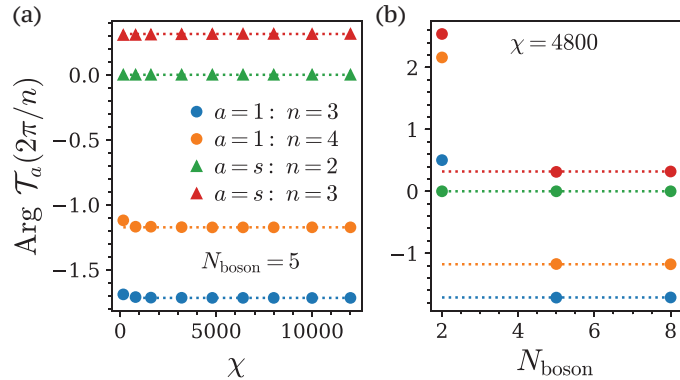


FIG. 8. Partial rotation $\mathcal{T}_a(2\pi/n)$ as a function of bond dimension χ and onsite boson number cutoff N_{Boson} at $L_y = 40\ell_B$. $\mathcal{T}_a(2\pi/n)$ saturates at relatively small $\chi = 1600$ and $N_{\text{Boson}} = 5$.

For readers who are familiar with the momentum polarization, we note that the precision required in the evaluation of $\mathcal{T}_a(\theta)$ is much higher in order to reliably extract the momentum polarization p_a due to the Hall viscosity term that is quadratic in cylinder circumference L_y . Specifically, the error in $\zeta_{n,a}$ and p_a are related to the error in $\text{Arg } \mathcal{T}_a(\theta)$ by

$$\Delta\zeta_{n,a} \sim \frac{\Delta \text{Arg } \mathcal{T}_a(\theta)}{\text{Arg } \mathcal{T}_a(\theta)}, \quad \Delta p_a \sim L_y^2 \frac{\Delta \text{Arg } \mathcal{T}_a(\theta)}{\text{Arg } \mathcal{T}_a(\theta)} \quad (60)$$

We note that $\zeta_{n,a}$ and p_a are both $O(1)$, but L_y^2 can be fairly large to avoid finite size effect. Therefore, a much smaller χ and N_{Boson} is required to reliably extract the higher central charge compared to that one would use for momentum polarization.

The main numerical challenge in our protocol to extract the higher central charge is the interpolating between higher central charge and momentum polarization discussed in an earlier section. We need to reach system size $L_y > n^2 \xi_r$ to reliably extract higher central charge $\zeta_{n,a}$. In quantum Hall systems, by comparing Eq. (9) and Eq. (59), we find

$$\xi_r = \sqrt{\frac{2\pi^2}{3}} \frac{c_-}{\nu \mathcal{S}} \ell_B = \sqrt{\frac{2}{3}} \pi \ell_B \quad (61)$$

where the last equality assumes the $\nu = 1/2$ bosonic Laughlin state. In order to obtain $\zeta_{n,a}$ with $n \geq 5$, we need to reach $L_y \geq 25 \sqrt{\frac{2}{3}} \pi \ell_B \approx 64\ell_B$, which can be challenging in practice.